

# Visualization of microvasculature and thrombi by X-ray phase-contrast computed tomography in hepatocellular carcinoma

Jianbo Jian,<sup>a</sup> Hao Yang,<sup>a</sup> Xinyan Zhao,<sup>b</sup> Ruijiao Xuan,<sup>a</sup> Yujie Zhang,<sup>c</sup> Dongyue Li<sup>d</sup> and Chunhong Hu<sup>a\*</sup>

Received 25 July 2015

Accepted 18 January 2016

Edited by P. A. Pianetta, SLAC National Accelerator Laboratory, USA

**Keywords:** hepatocellular carcinoma (HCC); microvasculature; thrombus; phase-contrast computed tomography (PCCT).

**Supporting information:** this article has supporting information at journals.iucr.org/s

<sup>a</sup>College of Biomedical Engineering, Tianjin Medical University, Tianjin 300070, People's Republic of China,

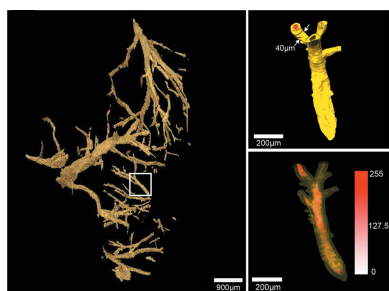
<sup>b</sup>Liver Research Center, Beijing Friendship Hospital, Capital Medical University, Beijing 100050, People's Republic of China, <sup>c</sup>Department of Pathology, Tianjin Medical University General Hospital, Tianjin 300052, People's Republic of China, and <sup>d</sup>School of Medical Imaging, Tianjin Medical University, Tianjin 300203, People's Republic of China.

\*Correspondence e-mail: chunhong\_hu@hotmail.com

Visualization of the microvascular network and thrombi in the microvasculature is a key step to evaluating the development of tumor growth and metastasis, and influences treatment selection. X-ray phase-contrast computed tomography (PCCT) is a new imaging technique that can detect minute changes of density and reveal soft tissues discrimination at micrometer-scale resolution. In this study, six human resected hepatocellular carcinoma (HCC) tissues were investigated with PCCT. A histological stain was added to estimate the accuracy of PCCT. The results showed that the fine structures of the microvasculature (measuring 30–100  $\mu\text{m}$ ) and thrombi in tiny blood vessels were displayed clearly on imaging the HCC tissues by PCCT. Moreover, density distributions of the thrombi were obtained, which could be reliably used to distinguish malignant from benign thrombi in HCC. In conclusion, PCCT can clearly show the three-dimensional subtle structures of HCC that cannot be detected by conventional absorption-based computed tomography and provides a new method for the imageology of HCC.

## 1. Introduction

Hepatocellular carcinoma (HCC) is the sixth most common tumor type and the third leading cause of cancer-related death worldwide (Bosch *et al.*, 1999). HCC usually arises in cirrhotic livers (Parkin *et al.*, 2005). The presence of malignant thrombi (tumor thrombi) serves as a crucial determinant of tumor staging, as well as prognosis, and influences treatment strategies (Takizawa *et al.*, 2007; Sakata *et al.*, 2008). Although surgical resection is one effective treatment for the disease, tumor recurrence in the remnant liver becomes unavoidable and uncontrollable if the malignant thrombi have reached beyond the extent of resection (Tsai *et al.*, 2000). Thus, the accurate visualization of malignant thrombi in hepatic vessels can promote an effective treatment strategy to reduce the risk of tumor recurrence. In recent years the possibility of using current clinical imaging modalities such as contrast-enhanced sonography, contrast-enhanced computed tomography (CT) and magnetic resonance imaging (MRI) to detect malignant thrombi in major vasculature has been reported (Okumura *et al.*, 1999; Ueno *et al.*, 2006; Shah *et al.*, 2007). However, there are still some difficulties in the observation and diagnosis of malignant thrombi in microvasculature. Firstly, microvasculature, and malignant thrombi in microvasculature, are beyond the detection limit of conventional angiography (Liu



© 2016 International Union of Crystallography

*et al.*, 2010). Secondly, malignant and benign (fibrin clot) thrombi can coexist in patients with cirrhosis and HCC (Ogren *et al.*, 2006; Sotiropoulos *et al.*, 2008). However, differentiating between benign and malignant thrombi in microvasculature is difficult without histological examination of the thrombus (Piscaglia *et al.*, 2010). Although the reference standard is pathologic examination, if performed improperly, tumor cells could be obtained from the adjacent HCC rather than from the thrombus, leading to misdiagnosis (Catalano *et al.*, 2010).

To overcome these challenges, a novel imaging method should be applied. Currently, X-ray phase-contrast imaging (PCI) is an emerging imaging technique that provides excellent image contrast for soft tissues (Davis *et al.*, 1995; Momose *et al.*, 1996). PCI, utilizing the phase shift, has approximately 1000 times greater sensitivity than conventional radiography (Momose *et al.*, 1996). Previous studies of PCI were mainly based on projections, which might omit the lesions hidden by superimposed structures (Takeda *et al.*, 1995; Lewis *et al.*, 2003). CT is a non-destructive technique widely used for visualizing interior features within samples, and for assessing quantitative information on their three-dimensional (3D) geometries and properties (Kak & Slaney, 2001). Fortunately, PCI has been successfully extended to CT mode recently, resulting in X-ray phase-contrast computed tomography (PCCT, also called PCI-CT in some studies) (Zysk *et al.*, 2012; Herzen *et al.*, 2014; Xuan *et al.*, 2015). In the technique of PCCT, hundreds or thousands of projections are acquired *via* PCI and subsequently reconstructed into CT slices using the filtered back-projection (FBP) algorithm (Duan *et al.*, 2013). Actually, PCCT is still based on the PCI technique and utilizes the phase shift as imaging signal. Thus, PCCT has the advantage of both PCI and CT in the detection of minute density changes in the soft tissues. Several applications of PCCT have already been reported. Microvasculature of hepatic fibrosis in rats (Hu *et al.*, 2009; Duan, Hu, Luo *et al.*, 2013) and sinusoid in human cavernous hemangioma of the liver (Duan *et al.*, 2013) have been clearly shown without contrast agents *via* PCCT. Moreover, due to the advantages of PCCT, visualization of the internal structures of microvasculature becomes possible and benign thrombi inside the microvasculature have already been displayed in 3D images (Zhang *et al.*, 2011; Duan, Hu, Luo *et al.*, 2013).

The value of PCCT has not, to our knowledge, been studied for characterizing microvasculature and intravascular thrombus in human HCC tissues. In this study, six HCC samples were used to perform the experiment without contrast agents *via* the PCCT technique. The aim of this study was to explore the potential of PCCT in microvasculature imaging for HCC tissues and to determine whether different types of thrombi at micrometer resolution could be differentiated based on PCCT images.

## 2. Materials and methods

### 2.1. Sample preparation

The project was designed as an *in vitro* experimental study. This study was approved by the ethics committee of Tianjin Medical University, Tianjin, China, and written informed consent was obtained from all patients. Six human HCC samples were prepared in the Department of Hepatobiliary Surgery, Tianjin Medical University Cancer Hospital. Patients had undergone hepatectomy without embolotherapy. The samples were cut into small pieces of 5 mm × 3 mm with a thickness of approximately 5 mm and fixed in 10% buffered formalin prior to imaging. During CT imaging, the samples were placed in cylindrical polyethylene containers, 6 mm in diameter. After imaging, the samples were imbedded in paraffin, and 4 μm-thick sections were cut and stained with hematoxylin and eosin (H&E). The histological sectioning and its corresponding analysis were accomplished by an experienced pathologist, and served as the reference standard for interpretation of the CT images of the HCC samples.

### 2.2. Image acquisition

All samples were imaged using the X-ray in-line PCI technique at beamline BL13W1 of the Shanghai Synchrotron Radiation Facility (SSRF) in China. A schematic of the experimental setup is shown in Fig. 1. The X-ray beam energy in the experiments was set at 20 keV, and the detector employed an X-ray CCD camera system with 9 μm × 9 μm pixels. One thousand two hundred projection images were obtained from each sample over 180° in rotation steps of 0.15°. The projections were recorded with a sample-to-detector

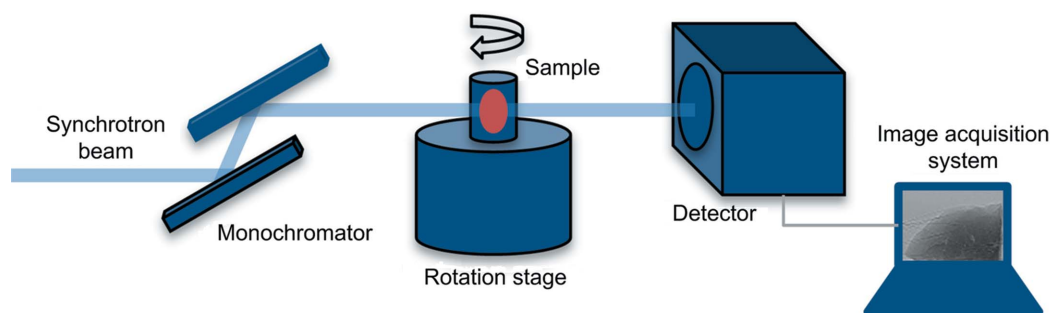


**Figure 1**

Schematic of the experiment setup. A monochromatic synchrotron X-ray beam is projected onto a sample fixed on a rotation stage, then the transmitted beam is recorded by an image detector and displayed by the image acquisition system. For tomographic scans, the stage can be rotated within 180° to acquire the projection images of the sample at different angles.

distance (SDD) of 1 m and exposure time of 10 ms. In addition, 20 flat-field images and ten dark-field images were collected.

### 2.3. Phase retrieval

The behavior of the X-rays while traversing a sample can be described by the 3D complex refractive index distribution,

$$n(x, y, z) = 1 - \delta(x, y, z) + i\beta(x, y, z), \quad (1)$$

where the real part  $\delta$  is the refractive index decrement and results in a phase shift; the imaginary  $\beta$  is the absorption index; and  $(x, y, z)$  are the spatial coordinates. Referring to (1), the obtained projection images display a mix of absorption information and phase information. Phase retrieval is a technique for obtaining quantitative phase information (*i.e.* the refractive index decrement  $\delta$ ) from obtained projection images. In general, phase retrieval requires at least two images, taken at two different SDDs (Nugent *et al.*, 1996). However, hundreds or thousands of projections will be taken in PCCT experiments. Taking PCCT data at two different SDDs will increase the exposure time and deliver a higher dose to the samples, which could hinder its biomedical applications (Burvall *et al.*, 2011). Therefore, a single-distance phase-retrieval algorithm, which only requires one CT data set obtained at a single SDD, has many advantages. Recently, several phase-retrieval algorithms using single-SDD PCCT data have been proposed (Gureyev *et al.*, 2004; Groso *et al.*, 2006). Phase retrieval employing only one-SDD PCCT data definitely makes the procedure much easier and will boost its applications, especially when the dose is an essential issue in the experiment. Moreover, comparison studies among phase-retrieval algorithms, utilizing single- and multi-SDD(s) PCCT data, have been conducted (Burvall *et al.*, 2011; Langer *et al.*, 2008; Yan *et al.*, 2011; Boone *et al.*, 2012), and these studies have proven that single-distance phase-retrieval methods also yield good results with the experimental data.

In our study, a single-distance phase-retrieval method, *i.e.* the phase-attenuation duality Born algorithm (PAD-BA), was used to extract the quantitative phase information. This method was proposed by Gureyev *et al.* (2004) and was designed for low- $Z$  and homogeneous materials. Later it was extended to tomography and applied to quasi-homogeneous objects such as soft tissues (Chen *et al.*, 2011). Since this method has been available for processing PCCT data, the studies cover both qualitative and quantitative investigation, such as 3D microvascular morphology investigation of rat liver (Xuan *et al.*, 2015), 3D visualization of an ant sample (Chen *et al.*, 2012) and 3D distribution of the real part of the refractive index reconstruction (Chen *et al.*, 2011). For this algorithm, *a priori* knowledge of the ratio  $\varepsilon$  between  $\delta$  and  $\beta$  of the refractive index is needed. Here we use  $\varepsilon = 1000$  at a SDD of 1 m for the HCC tissues, and this value has been considered a typical ratio for the soft tissues in some other experiments (Chen *et al.*, 2011; Xuan *et al.*, 2015). Thus, the 3D quantitative phase information reconstruction *via* PCCT was based on a two-step approach: first, the phase information was extracted

from the projection images by the PAD-BA, and then the 3D distribution of the phase information was reconstructed by applying the standard FBP algorithm. Moreover, the reconstructed phase information is proportional to the density distribution of the sample (Willner *et al.*, 2013; Hoshino *et al.*, 2014). Thus, PCCT images after phase retrieval are particularly suitable for quantitative density evaluation.

### 2.4. Image reconstruction and 3D visualization

Projection images were taken with flat-field and dark-field correction, and the single-distance phase-retrieval method, *i.e.* PAD-BA, was utilized to extract the phase information. Then, the phase images were reconstructed using a standard FBP algorithm. The 3D microstructures of the HCC were visualized using *Amira 5.2* software (Visage Imaging, Berlin, Germany), which allowed a clear 3D visualization of the anatomical and pathological features of the microvasculature.

## 3. Results

### 3.1. X-ray CT imaging and histopathologic analysis

Fig. 2(a) shows the histological result obtained with H&E staining and Fig. 2(c) shows a CT image of the samples. These two findings are very similar. Based on matching of outstanding characteristics (arrows), a good correlation

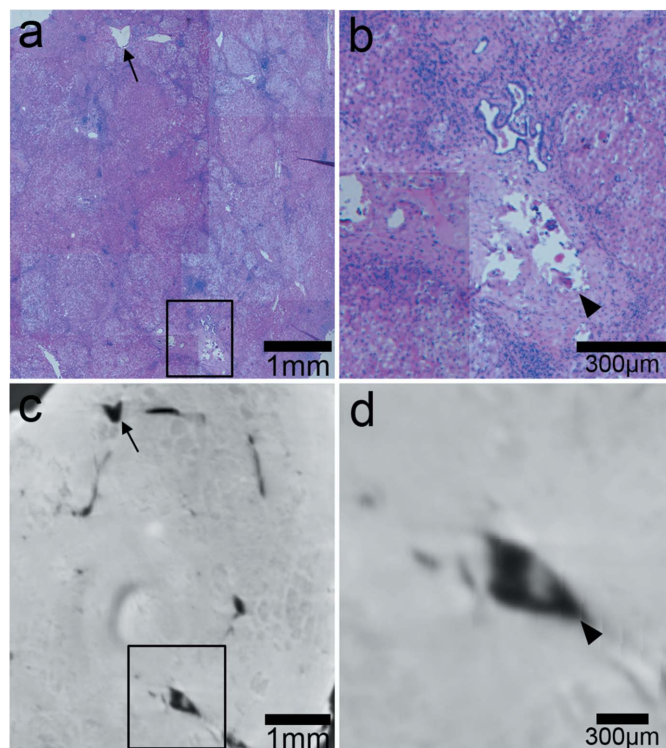


**Figure 2** Comparison of imaging results (axial tomography slices) and the corresponding histological slice obtained from the HCC samples. (a) Histological section. (c) CT image. (b) and (d) are magnified images of the black rectangle regions in (a) and (c), respectively. Black arrows: vessels. Black arrow heads: malignant thrombi.

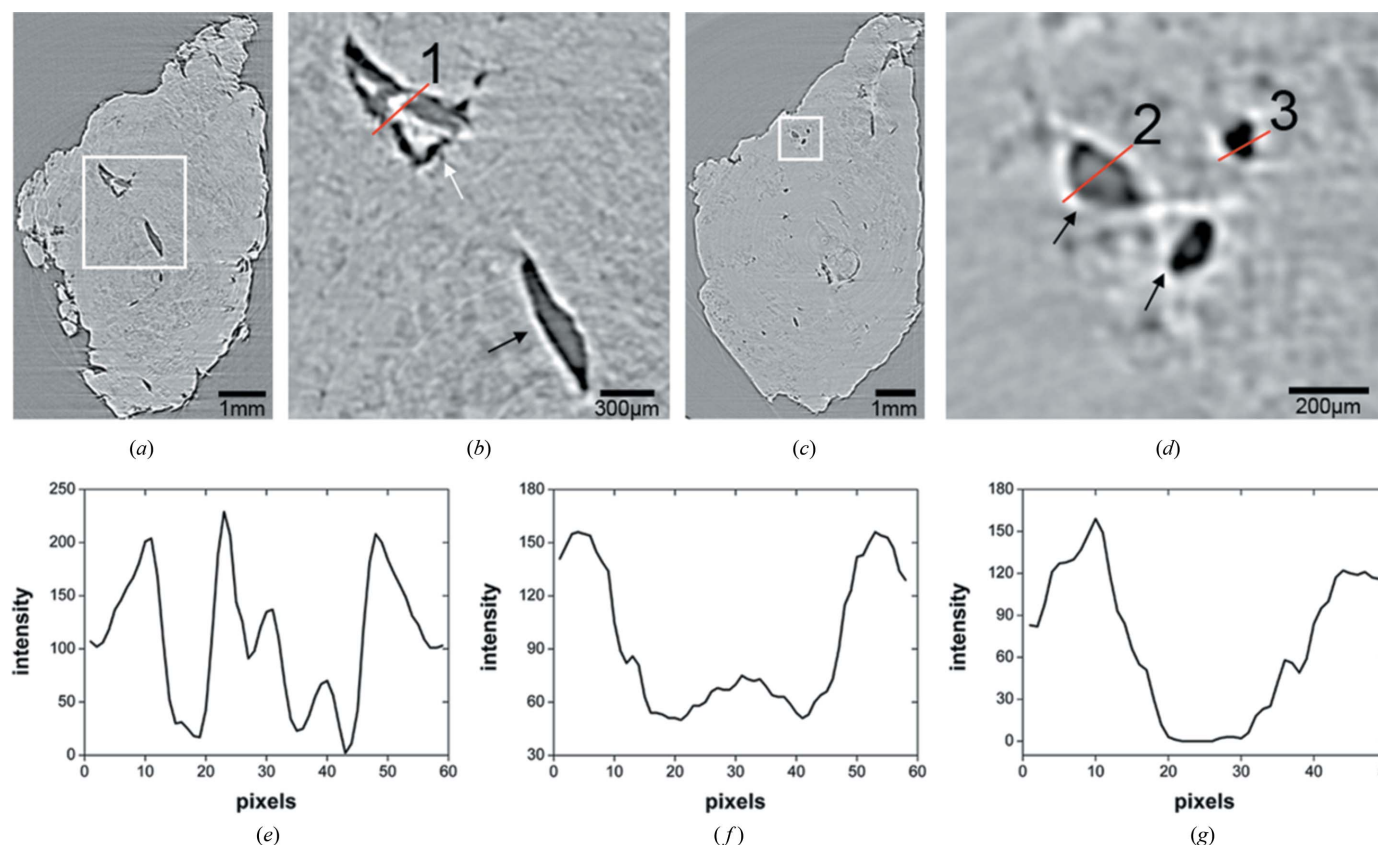


**Figure 3**

Slices with thrombi and density distributions of the thrombi. (a) and (c) are slices with thrombi. (b) and (d) are magnified images of the white rectangle regions in (a) and (c), respectively. (e) Profile of the red line numbered 1 in (b). (f) Profile of the red line 2 in (d). (g) Profile of the red line 3 in (d). White arrow: benign thrombus. Black arrows: malignant thrombi.

between CT images and the histological sections was demonstrated, especially for the vessels with diameters of less than  $200\ \mu\text{m}$  (black arrows). The malignant thrombi (black arrow heads) in microvasculature were clearly visible in the CT image.

### 3.2. Differentiation of malignant from benign thrombi via density distribution

Fig. 3 shows CT images and density distributions of thrombi in HCC tissues by PCCT. Figs. 3(a)–3(d) display thrombi (arrows) in microvasculature and density profiles of the thrombi are shown in Figs. 3(e)–3(g). Benign thrombi were made up of fibrin, which expressed a non-uniform density distribution and sometimes had a higher density than the vascular walls caused by calcium deposits, as shown in Figs. 3(b) (white arrow) and 3(e). In contrast, malignant thrombi mainly consisted of tumor cells, so the density would be equally distributed and lower than the blood vessel walls, as shown in Figs. 3(d) (black arrows) and 3(f). Additionally, Figs. 3(d) (line 3) and 3(g) show that the density in normal vessels was close to zero.

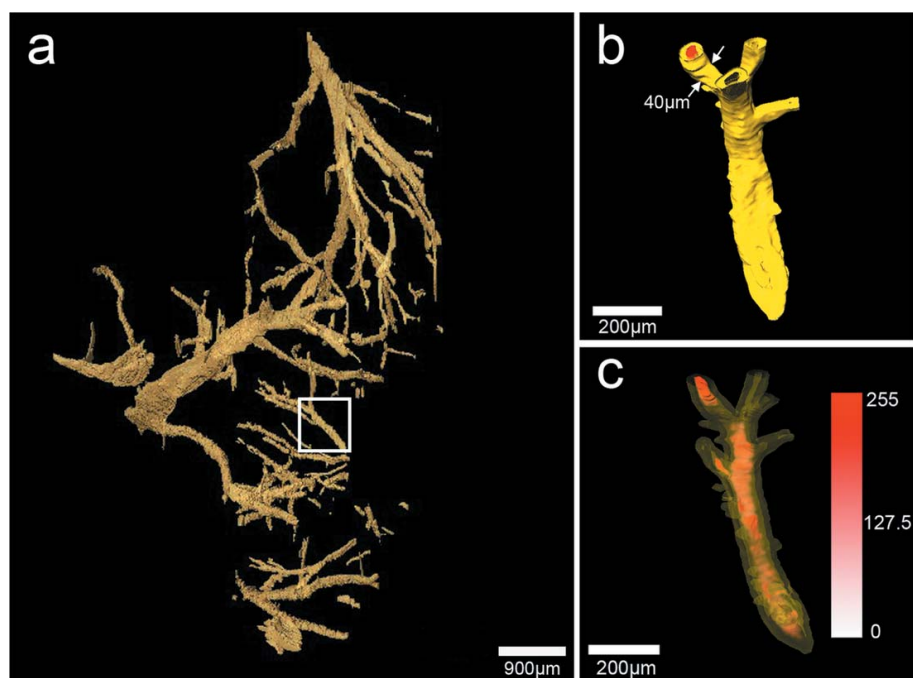
### 3.3. 3D visualization of microvasculature and thrombi

Fig. 4 shows 3D microvasculature images of HCC. The network of hepatic blood vessels could be observed clearly in

Fig. 4(a) and the smallest visible vessels were approximately  $30\text{--}40\ \mu\text{m}$  in diameter [marked by white arrows in Fig. 4(b)]. For better visualization of the vessel, the 3D model could be rotated in real time (see Video S1 of the supporting information). Figs. 4(b) and 4(c) present 3D structures of the thrombi, and the 3D reconstruction videos are also provided in the supporting data (Videos S2 and S3). In Fig. 4(c), the vascular walls were made transparent so that the inner of the vessels could be clearly presented. As can be seen, the upper parts were benign thrombi with a high density, and the lower parts were malignant thrombi with a low and equally distributed density.

## 4. Discussion

Our PCCT experiment on HCC samples at the beamline BL13W1 of the SSRF demonstrates that PCCT can clearly depict the 3D structure of the microvascular network (smallest diameter between  $30$  and  $40\ \mu\text{m}$ ) and thrombi in microvasculature. Moreover, the PCCT images are found to be consistent with histological sections. By utilizing phase retrieval, density distributions of the thrombi make it possible to distinguish malignant thrombi (tumor cells) from benign thrombi (fibrin clot, often accompanied by calcium deposits) in HCC.



**Figure 4**  
 (a) 3D vessel microstructure image of HCC. (b) and (c) are magnified images of the region in the white box in (a). (b) Surface reconstruction image. (c) Volume rendering image. The color bar on the right represents the density of the relative thrombi area, and graded levels from white to red indicate an increase in the density.

PCCT is a new imaging technique that can detect minute changes of density and reveal soft tissues discrimination at micrometer-scale resolution (Duan *et al.*, 2013). By means of the PCCT technique, imaging of murine HCC has been developed by the investigators (Tao *et al.*, 2012), but the study of human HCC imaging has rarely been reported before. The study has demonstrated that PCCT can present an accurate morphology of the microstructures in HCC tissues by comparing CT image with histological section. Visualization of the microvasculature is an important step to understand mechanisms of tumor growth and develop effective therapeutic strategies (Liu *et al.*, 2010). However, microvasculature involved in HCC is beyond the detection limit of conventional angiography. In this study, the network of microvasculature in HCC tissues could be clearly observed *via* PCCT, and the 3D structure and diameters of the microvasculature were studied. The smallest visible vessels were approximately 30–40  $\mu\text{m}$  in diameter. The results show that it is feasible to image microvasculature in human HCC tissues using PCCT. In addition, malignant thrombus is a contraindication for liver transplantation in HCC (Piscaglia *et al.*, 2010), especially for the malignant thrombus in microvasculature which cannot be detected by current clinical imaging modalities but may cause tumor recurrence after liver transplantation. Due to the development of the PCCT, detection of thrombi in the microvasculature becomes possible. In this paper, the 3D structure of the thrombi in microvasculature is clearly observed using PCCT. However, patients with cirrhosis and HCC may have either malignant or benign thrombi, and differentiating between malignant

and benign thrombi is difficult without histological examination of the thrombus. Moreover, benign and malignant thrombi are formed through different pathophysiological mechanisms with differing density distribution. Benign thrombus, which develops from sluggish blood flow, is characterized by blood clots or fibrin without viable cells (Piscaglia *et al.*, 2010) and may show calcium deposits (Catalano *et al.*, 2011). This type of thrombus will display a high density distribution. Conversely, malignant thrombi, which are often caused by the direct invasion of HCC into the hepatic vasculature (Lee *et al.*, 2008), are associated with a lower density distribution compared with benign thrombi. Thus, the difference in the density distribution can be utilized to differentiate between malignant and benign thrombi. Recently, the single-distance phase-retrieval method has been developed (Chen *et al.*, 2011) and small density differences can be clearly visualized *via* PCCT images after phase retrieval (Hoshino *et al.*, 2014). Therefore,

the present study has successfully utilized density distribution to discriminate malignant from benign thrombi in PCCT images after phase retrieval, which will be greatly helpful to accurately detect malignant thrombi in the microvasculature.

It is noteworthy that the PCCT technique provides a novel and promising approach for the direct visualization of microstructure in HCC tissues. However, there are still some limitations in PCCT. Above all, compared with the clinical technology, the setup we used for the current study was limited to a small field of view, which is not suited for imaging large samples. Actually, a recent study has shown that PCCT can allow the visualization of breast tissues structures and abnormalities in a large field of view (Sztrókay *et al.*, 2012). Secondly, *in vivo* PCCT still remains a challenge; we designed this *in vitro* study in order to investigate the possibility for future use. Finally, current PCCT experiments are mostly performed using synchrotron radiation, which hinders its potential clinical application. Recently, PCCT techniques using a conventional X-ray tube have been developed, which will be an important step towards the clinical implementation of PCCT (Hetterich *et al.*, 2014).

In conclusion, PCCT can clearly depict tiny blood vessels in the HCC tissues and thrombi in microvasculature without the help of a contrast agent. Demonstrations of the fine structure of thrombi and microvasculature and the differentiation of malignant from benign thrombi *via* density distribution all provide useful information for the diagnosis of HCC. Although this technique is presently not applicable in clinical practice, the potential for its application demonstrated by this

research may provide a new direction for the future imaging of HCC.

### Acknowledgements

This work was supported by the National Natural Science Foundation of China (Grant Nos. 81371549, 30900333 and 81000178), the WBE Liver Fibrosis Foundation of China (Grant No. CFHPC20131033), and the Science Fund of Tianjin Medical University (Grant No. 2011KY46). The authors would like to thank the staff from beamline (BL13W1) of SSRF, China, for their kindly assistance during the experiments.

### References

- Boone, M. N., Devulder, W., Dierick, M., Brabant, L., Pauwels, E. & Van Hoorebeke, L. (2012). *J. Opt. Soc. Am. A*, **29**, 2667–2672.
- Bosch, F. X., Ribes, J. & Borràs, J. (1999). *Semin. Liver Dis.* **19**, 271–285.
- Burvall, A., Lundström, U., Takman, P. A., Larsson, D. H. & Hertz, H. M. (2011). *Opt. Express*, **19**, 10359–10376.
- Catalano, O. A., Choy, G., Zhu, A., Hahn, P. F. & Sahani, D. V. (2010). *Radiology*, **254**, 154–162.
- Catalano, O., Nunziata, A., de Lutio di Castelguidone, E. & d'Errico, A. G. (2011). *Acta Radiol.* **52**, 730–737.
- Chen, R.-C., Dreossi, D., Mancini, L., Menk, R., Rigon, L., Xiao, T.-Q. & Longo, R. (2012). *J. Synchrotron Rad.* **19**, 836–845.
- Chen, R. C., Rigon, L. & Longo, R. (2011). *J. Phys. D*, **44**, 495401.
- Davis, T., Gao, D., Gureyev, T., Stevenson, A. & Wilkins, S. (1995). *Nature (London)*, **373**, 595–598.
- Duan, J., Hu, C. & Chen, H. (2013). *PLoS One*, **8**, e53507.
- Duan, J., Hu, C., Luo, S., Zhao, X. & Wang, T. (2013). *PLoS One*, **8**, e78176.
- Groso, A., Abela, R. & Stampanoni, M. (2006). *Opt. Express*, **14**, 8103–8110.
- Gureyev, T. E., Davis, T. J., Pogany, A., Mayo, S. C. & Wilkins, S. W. (2004). *Appl. Opt.* **43**, 2418–2430.
- Herzen, J., Willner, M. S., Fingerle, A. A., Noël, P. B., Köhler, T., Drecoll, E., Rummeny, E. J. & Pfeiffer, F. (2014). *PLoS One*, **9**, e83369.
- Hetterich, H., Willner, M., Fill, S., Herzen, J., Bamberg, F., Hipp, A., Schüller, U., Adam-Neumair, S., Wirth, S., Reiser, M., Pfeiffer, F. & Saam, T. (2014). *Radiology*, **271**, 870–878.
- Hoshino, M., Uesugi, K., Tsukube, T. & Yagi, N. (2014). *J. Synchrotron Rad.* **21**, 1347–1357.
- Hu, C., Zhao, T., Zhang, L., Li, H., Zhao, X. & Luo, S. (2009). *Prog. Nat. Sci.* **19**, 955–962.
- Kak, A. C. & Slaney, M. (2001). *Principles of Computerized Tomographic Imaging*. Philadelphia: Society of Industrial and Applied Mathematics.
- Langer, M., Cloetens, P., Guigay, J. P. & Peyrin, F. (2008). *Med. Phys.* **35**, 4556–4566.
- Lee, H. K., Park, S. J., Yi, B. H., Yeon, E. K., Kim, J. H. & Hong, H. S. (2008). *Abdom. Imaging*, **33**, 72–79.
- Lewis, R. A., Hall, C. J., Hufton, A. P., Evans, S., Menk, R. H., Arfelli, F., Rigon, L., Tromba, G., Dance, D. R., Ellis, I. O., Evans, A., Jacobs, E., Pinder, S. E. & Rogers, K. D. (2003). *Br. J. Radiol.* **76**, 301–308.
- Liu, P., Sun, J., Zhao, J., Liu, X., Gu, X., Li, J., Xiao, T. & Xu, L. X. (2010). *J. Synchrotron Rad.* **17**, 517–521.
- Momose, A., Takeda, T., Itai, Y. & Hirano, K. (1996). *Nat. Med.* **2**, 473–475.
- Nugent, K. A., Gureyev, T. E., Cookson, D. J., Paganin, D. & Barnea, Z. (1996). *Phys. Rev. Lett.* **77**, 2961–2964.
- Ogren, M., Bergqvist, D., Björck, M., Acosta, S., Eriksson, H. & Sternby, N. H. (2006). *World J. Gastroenterol.* **12**, 2115–2119.
- Okumura, A., Watanabe, Y., Dohke, M., Ishimori, T., Amoh, Y., Oda, K. & Dodo, Y. (1999). *Radiographics*, **19**, 973–987.
- Parkin, D. M., Bray, F., Ferlay, J. & Pisani, P. (2005). *CA Cancer J. Clin.* **55**, 74–108.
- Piscaglia, F., Cucchetti, A., Terzi, E. & Gianstefani, A. (2010). *Liver Transpl.* **16**, 1006–1007.
- Sakata, J., Shirai, Y., Wakai, T., Kaneko, K., Nagahashi, M. & Hatakeyama, K. (2008). *Eur. J. Surg. Oncol.* **34**, 900–905.
- Shah, Z. K., McKernan, M. G., Hahn, P. F. & Sahani, D. V. (2007). *Am. J. Roentgenol.* **188**, 1320–1323.
- Sotiropoulos, G. C., Radtke, A., Schmitz, K. J., Molmenti, E. P., Schroeder, T., Saner, F. H., Baba, H. A., Fouzas, I., Broelsch, C. E., Malagó, M. & Lang, H. (2008). *Dig. Dis. Sci.* **53**, 1994–1999.
- Sztrókay, A., Diemoz, P. C., Schlossbauer, T., Brun, E., Bamberg, F., Mayr, D., Reiser, M. F., Bravin, A. & Coan, P. (2012). *Phys. Med. Biol.* **57**, 2931–2942.
- Takeda, T., Momose, A., Itai, Y., Jin, W. & Hirano, K. (1995). *Acad. Radiol.* **2**, 799–803.
- Takizawa, D., Kakizaki, S., Sohara, N., Sato, K., Takagi, H., Arai, H., Katakai, K., Kojima, A., Matsuzaki, Y. & Mori, M. (2007). *Dig. Dis. Sci.* **52**, 3290–3295.
- Tao, Q., Li, D., Zhang, L. & Luo, S. (2012). *PLoS One*, **7**, e39936.
- Tsai, T.-J., Chau, G.-Y., Lui, W.-Y., Tsay, S.-H., King, K.-L., Loong, C.-C., Hsia, C.-Y. & Wu, C.-W. (2000). *Surgery*, **127**, 603–608.
- Ueno, N., Kawamura, H., Takahashi, H., Fujisawa, N., Yoneda, M., Kirikoshi, H., Sakaguchi, T., Saito, S. & Togo, S. (2006). *J. Ultrasound Med.* **25**, 1147–1152.
- Willner, M., Bech, M., Herzen, J., Zhanette, I., Hahn, D., Kenntner, J., Mohr, J., Rack, A., Weitkamp, T. & Pfeiffer, F. (2013). *Opt. Express*, **21**, 4155–4166.
- Xuan, R., Zhao, X., Hu, D., Jian, J., Wang, T. & Hu, C. (2015). *Sci. Rep.* **5**, 11500.
- Yan, A., Wu, X. & Liu, H. (2011). *Med. Phys.* **38**, 5073–5080.
- Zhang, L., Hu, C., Zhao, T. & Luo, S. (2011). *Eur. J. Radiol.* **80**, 158–162.
- Zysk, A. M., Garson, A. B., Xu, Q., Brey, E. M., Zhou, W., Brankov, J. G., Wernick, M. N., Kuszak, J. R. & Anastasio, M. A. (2012). *Biomed. Opt. Express*, **3**, 1924–1932.